Impact wear and mechanical behavior of steels at subzero temperatures

Kati Valtonen*, Vilma Ratia[1], Karthik Ram Ramakrishnan, Marian Apostol, Juuso Terva, Veli-Tapani Kuokkala

Tampere University of Technology, Laboratory of Materials Science, Tampere Wear Center, P.O. Box 589, FI-33101, Tampere, Finland

ARTICLE INFO

ABSTRACT

In this study, the deformation behavior of three steels was studied at Arctic temperatures by controlled single and multiple oblique angle impacts. The results were compared with the mechanical properties of the steels determined at the corresponding temperatures. At subzero temperatures, the hardness and strength of the studied steels increased and their ability to deform plastically steadily decreased. In the martensitic steels, adiabatic shear bands were observed to form during the impacts at subzero temperatures, indicating that the deformation ability of the steels was critically impaired. At $-60\,°C$, the adiabatic shear bands commonly acted as initiation sites for subsurface cracks. Moreover, the surface characterization of the test samples revealed formation of cracks and wear particles, which was connected to the opening of grain boundaries and martensite laths at low temperatures. Finite Element Modeling was also used to obtain more information about the impact event.

1. Introduction

When the temperature of the operating environment is lowered, unforeseen behavior of materials may lead to serious problems for example in Arctic mining, where the challenges created by wear and subzero temperatures easily combine and amplify [1]. According to a report describing the behavior of mining tools during winter in Yakutia, Siberia, "steel tools became so brittle that they broke like match sticks" [2].

Ferritic structural steels and martensitic high-strength steels are widely used materials for construction and machinery, but their body-centered cubic microstructure makes them susceptible to ductile-to-brittle transition (DBT) at low temperatures, where an otherwise relatively ductile material begins to behave in a brittle manner. In practice, this means that operating the machinery at a too low temperature may be a cause for an unexpected failure.

The DBT problems are well recognized in the ship building industry, which now has strict policies and standards for material testing, welding, and design to avoid catastrophic failures such as those of the Liberty ships during World War II [3]. With the widening interest of utilizing the resources in the Arctic, combined with the concern on its environmental impact, also the Arctic offshore structures and building materials have been studied and the critical material characteristics and welding requirements have been considered [4–7].

While the design and welding parameters of steel structures are

important, the effect of wear on the materials should not be neglected, since it also affects the long-term endurance and stability of the structures, and in a shorter term, the endurance of different types of machinery with a direct effect on the reliability and productivity of the industry. Testing of the low temperature impact properties of steels is typically done using the standardized tests, such as the Charpy pendulum impact tests [8] and the drop-weight tests [9]. For the testing of steels under high strain rates, the Hopkinson Split Bar method with a cooling system has been successfully utilized [10–12]. Some tribological testing related to cryogenic and space applications have been conducted under sliding conditions [13,14]. Recently also some studies of the effects of low outdoor temperatures on the wear behavior of materials in the wheel-rail contacts have been published [15,16]. Moreover, Ratia et al. [17] studied single impacts on a martensitic steel at temperatures down to $-60\,°C$ using the High Velocity Particle Impactor (HVPI) method, which enables studying in particular the early stages of impact wear at Arctic conditions [17].

Adiabatic shear bands (ASB) can form in martensitic steels when they are subjected to high velocity impacts or plastic deformation at high strain rates [18–21]. The ASBs are formed by a process where localized plastic deformation leads to an increase of temperature and austenization of the steel followed by rapid cooling and formation of untempered martensite [19,22]. The transformed ASBs are seen as white etching bands in optical micrographs with a very fine microstructure and a higher hardness than the original bulk material [21]. In

---

* Corresponding author.
  E-mail address: kati.valtonen@tut.fi (K. Valtonen).
[1] Current location: Faculty of Engineering, University of Nottingham, University Park, Nottingham NG7 2RD, UK.
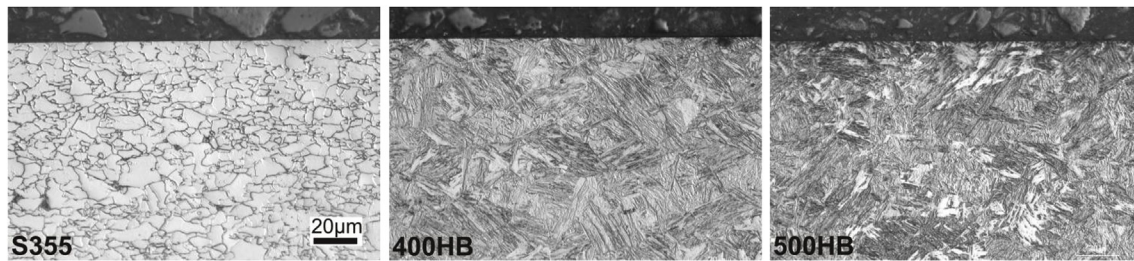
Fig. 1. Initial microstructures of the tested steels.

Table 1
Nominal compositions of the studied steels.

Steel	S355	400HB	500HB
Microstructure	Ferritic-pearlitic	Martensitic	Martensitic
C [wt%] max.	0.12	0.23	0.30
Si [wt%] max.	0.03	0.80	0.80
Mn [wt%] max.	1.5	1.70	1.7
Cr [wt%] max.	–	1.5	1.5
Ni [wt%] max.	–	1.0	1.0
Mo [wt%] max.	–	0.5	0.5
B [wt%] max.	–	0.005	0.005

high stress impacts, the transformed ASBs may also act as initiation sites of cracks [21,23,24]. However, the deformed ASBs, which appear as dark lines when the etched surface is studied with an optical microscope, have not been reported to show cracking [21].

With the improvements in computational capabilities, numerical simulations can now be more efficiently utilized to study also the complex mechanical and thermal interactions encountered in various wear processes [25]. Consequently, modeling is becoming an indispensable tool in the rapid implementation of novel sustainable tribology to practical engineering problems [26]. In addition to providing a cost effective and fast tool for iterating and optimizing the material wear properties, the numerical models enhance the exploitation of the results of experimental wear testing. There are several published articles about the simulation of impacting steel targets, including for example the papers by Arias et al. [27] and Iqbal et al. [28]. However, the focus of these models was on ballistic impacts and penetration and not on the impact wear phenomena at subzero temperatures. Cho et al. [29]

simulated the low temperature impacting of steels, but the study concentrated on low velocity impact testing with a drop tower.

In order to understand better the effects of subzero temperatures on the impact wear behavior and microstructural changes of steels due to deformation at relatively high impact energies, two wear resistant steels and a construction steel were tested and characterized. The results were compared with the mechanical properties of the studied steels. Moreover, the response of the steels to impacts was studied using numerical simulations.

2. Materials and methods

2.1. Materials

The materials selected for the tests include two martensitic wear resistant steels, denoted as 400HB and 500HB based on their hardness grades and a ferritic-pearlitic structural steel S355 used as a reference material. Fig. 1 presents the initial microstructures of the tested materials, and Table 1 lists their typical compositions.

2.2. Methods

The High Velocity Particle Impactor is a test device developed for single and multiple impact wear testing at Tampere Wear Center [30]. The HVPI system enables controlled shooting of single 9 mm projectiles to a tilted target material with a temperature ranging from room temperature down to ca. −100 °C. The impact velocity can be as high as 165 m/s, depending on the mass of the projectile that is shot through a smooth bore using pressurized air [31]. The samples are cooled by nitrogen gas flowing through a heat exchanger immersed in liquid nitrogen. Fig. 2 presents a schematic of the HVPI with the cooling system,
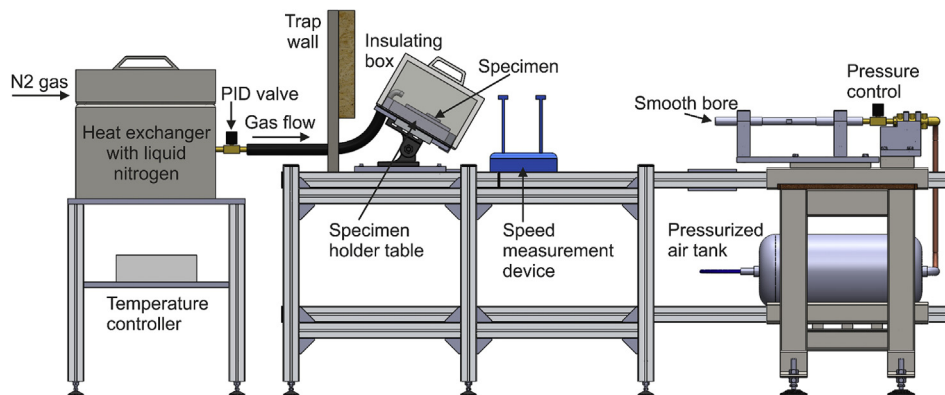

Fig. 2. Schematic of the high velocity particle impactor (HVPI) with a cooling system.

Table 2
Test parameters used in the high velocity particle impactor tests and the mechanical tests.

|	HVPI	Charpy	Tensile	Hardness
Test temperatures (*only for 500HB steel)	RT, −20 °C, −60 °C (1 °C, −1 °C)*	40 °C, RT, −20 °C, −40 °C, −60 °C, −70 °C, −80 °C	RT, −20 °C, −40 °C, −60 °C	RT, −60 °C, −100 °C, (-150 °C)*
Test type	Projectile impact test	V-notch	Servohydraulic materials testing machine	Vickers HV10
Impact velocity [m/s]	110–114			
Sample angle [°]	60			
Sample size [mm]	40 × 40 x 4	5 × 10 x 55	5 × 8 x 70 (5 × 8 x 75 at RT)	40 × 40 x 4
Projectile	WC-Co bearing ball			
Projectile diameter [mm]	9			
Projectile weight [g]	5.7			
Nominal energy of projectile/pendulum [J]	35–37	300		
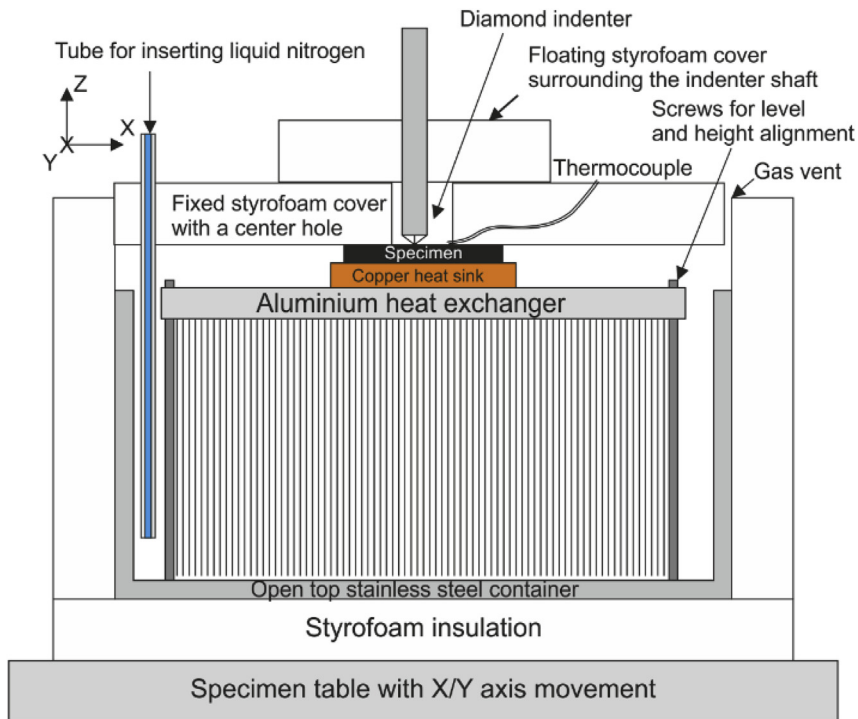
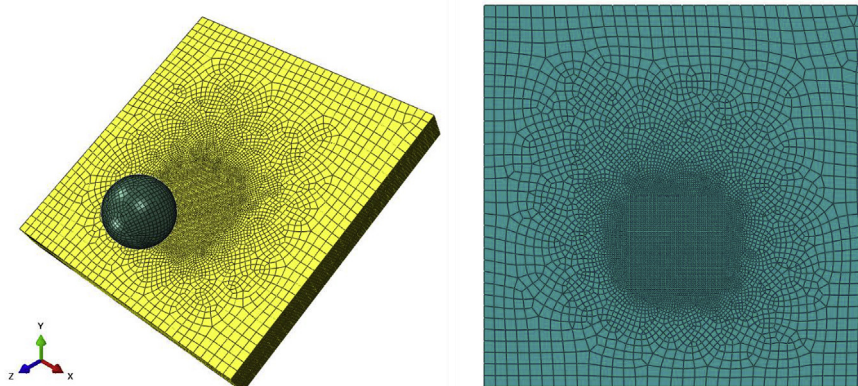**Fig. 3.** Schematic of the low temperature hardness testing system.

Fig. 4. Finite element model for the simulation of the HVPI steel target.

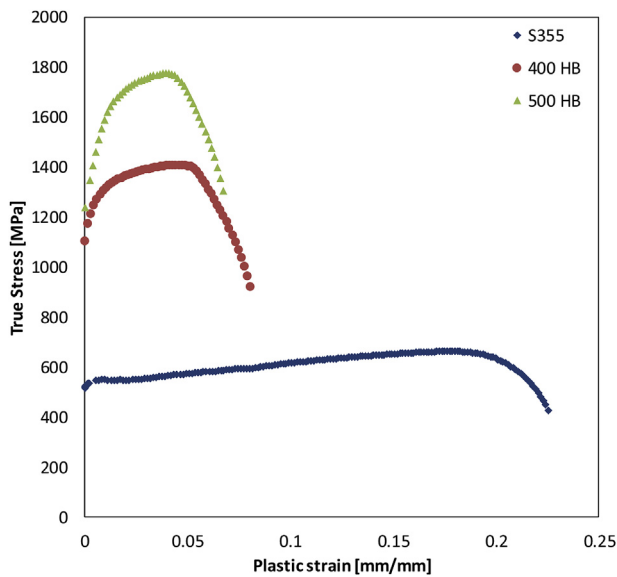**Fig. 5.** Post-yield behavior of the 400HB, 500HB and S355 steels at −60 °C used for the FE material models.

which is described in more details by Ratia et al. in Ref. [17]. A similar cooling system has been used earlier for the low temperature Hopkinson Split Bar tests [10]. Before the test, the insulating box is removed and the temperature is let to stabilize for a few minutes to reach the desired test temperature.

In this study, the temperatures of the impacted test materials were room temperature (RT, 22–23 °C), −20 °C, and −60 °C, and the impact velocity of 110–114 m/s and an impact angle of 60° were applied. The selected impact velocity provides the highest possible impact energy, 35–37 J, with WC-Co projectiles [18]. Three separate impacts were made with 9 mm spherical WC-Co (ISO K20 with 6% Co) projectiles under each condition. The projectiles were at room temperature. Before the tests, the surfaces of the 40 × 40 × 4 mm samples were polished with 1 μm diamond paste and two K-type thermocouples were spot-welded on them to measure the temperature of the sample surfaces. The samples were cooled a few degrees below the target temperature and kept there for a few minutes to even out the temperature before the actual test. The ice formed from the condensed air moisture was wiped off with a cotton cloth just before the impact. Table 2 lists the testing parameters of the used test methods.

To study the effect of multiple impacts, the 500HB steel was

impacted five times at RT, −20 °C, and −60 °C. The samples were always re-cooled between the impacts. The 500HB steel was tested also at +1 °C and −1 °C to study the effect of the ice layer formation on the impact test outcome. The −1 °C samples were first cooled down to −20 °C and kept there for about 5 min. After that, the cooling was turned off, the insulating box was lifted off, and the sample was let to warm up to the impact temperature. The visibly thick frost layer was not wiped off prior to testing as in the other tests. For the tests at +1 °C, the sample surfaces were wiped dry with a cotton cloth and impacted right after the temperature had raised above the zero temperature. However, water condensation on the cold surfaces was quite rapid, and it was likely that at least a thin film of water was present on the surfaces already at the time of the impact.

The surfaces of the tested samples were characterized using Zeiss UltraPlus field emission scanning electron microscope (SEM), Leica MZ 7.5 zoom stereo microscope, and Alicona G5 InfiniteFocus 3D profiler. Furthermore, the microstructural changes and the deformed layers were studied from the longitudinal cross-sections of the impact marks with Nikon Eclipse MA 100 optical microscope. The cross sections were prepared from the longitudinal middle sections of the impact scars using standard metallographic methods, including etching with 4% Nital.

The mechanical tests, including Charpy V-notch pendulum impact tests and tensile tests at low temperatures, were conducted by the steel manufacturer in controlled temperature chambers cooled with liquid nitrogen. The temperature was measured with a thermocouple attached to the sample. Charpy V-notch pendulum impact tests [8] were made at 40 °C, 20 °C, −20 °C, −40 °C, −60 °C, −70 °C, and −80 °C in the parallel and transverse directions relative to the rolling direction. The sample size was 5 mm × 10 mm x 55 mm. The tensile tests were made at RT, −20 °C, −40 °C, and −60 °C using the sample size of 5 mm × 8 mm x 70 mm produced in the rolling direction. In the room temperature tests, however, the parallel sample length (L_c) was 75 mm.

For the low temperature hardness testing, an insulated heat exchanger was designed and built on a mechanical Zwick Vickers hardness system, as illustrated in Fig. 3. The HV10 indentations were made in the polished sample surfaces in the chamber but the dimensions were measured at room temperature with an optical microscope. The effect of thermal expansion on the measured values was determined to be less than 1 HV at −60 °C. The microhardness testing of the deformed layers was performed as $HV_{0.025}$ (254.2 mN) using Matsuzawa MMT-X7 micro Vickers hardness tester at RT.

2.3. Finite element analysis

The response of steel plates to high velocity particle impacts was

Table 3
Measured mechanical properties of the studied steels at the HVPI test temperatures.

| Material (temperature)	Rp0.2 [MPa]	Rm [MPa]	A_5 [%]	Charpy V [J] longitudinal	Charpy V [J] transverse	Hardness [HV_{10}]
S355 (RT)	421 ± 3	492 ± 1	33.5 ± 0.5	94 ± 3	77 ± 2	164 ± 1.5
S355 (−20 °C)	456 ± 3	527 ± 1	35.5 ± 0.4	108 ± 2	80 ± 1	
S355 (−60 °C)	526 ± 2	560 ± 2	36.5 ± 0.2	85 ± 8	58 ± 3	182 ± 1.8
400HB (RT)	1099 ± 17	1247 ± 8	12.9 ± 0.2	53 ± 1	42 ± 0	401 ± 1.5
400HB (−20 °C)	1117 ± 3	1309 ± 11	14.6 ± 0.3	37 ± 9	29 ± 3	
400HB (−60 °C)	1153 ± 11	1328 ± 23	14.4 ± 0.6	13 ± 6	7 ± 4	415 ± 2.8
500HB (RT)	1329 ± 19	1653 ± 15	10.5 ± 0.3	26 ± 2	18 ± 2	506.5 ± 6.5
500HB (−20 °C)	1299 ± 90	1678 ± 3	11.6 ± 0.3	16 ± 2	15 ± 2	
500HB (−60 °C)	1303 ± 39	1700 ± 5	12.2 ± 0.4	11 ± 1	10 ± 1	535 ± 12.1

a) *b)*
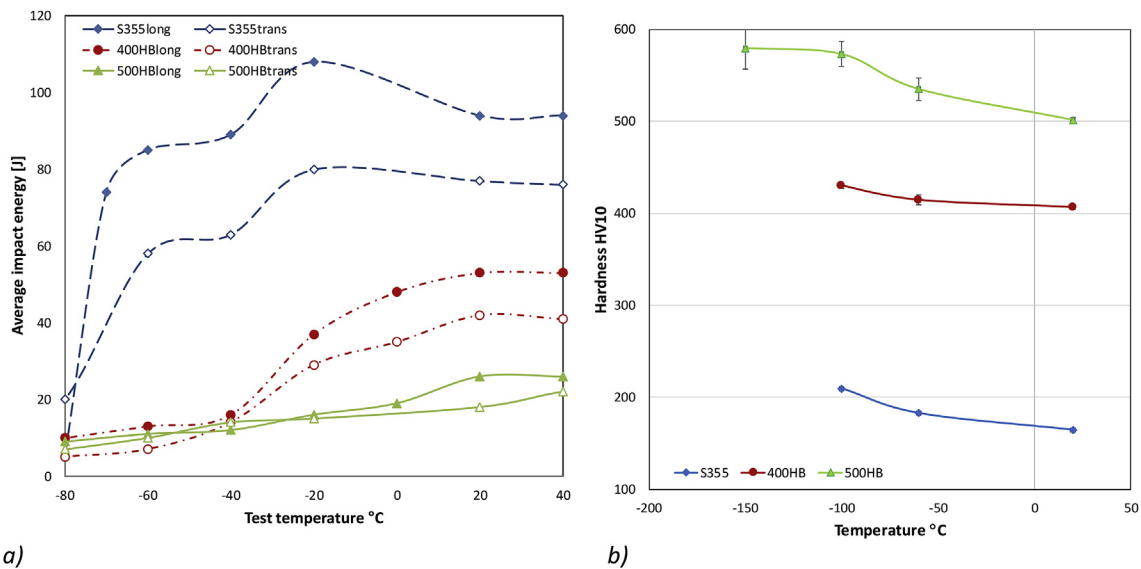
Fig. 6. A) Charpy V impact energy values at different temperatures in the longitudinal (long, sample prepared in the rolling direction) and transverse (trans) directions with a 5 mm × 10 mm x 55 mm sample size, and b) Vickers hardness values of the studied steels as a function of temperature (error bars present the standard deviation).

also examined using Finite Element (FE) analysis with Abaqus/Explicit. The experimental setup, including the target plate and the projectile, was replicated in the FE model. The square plates of 40 mm × 40 mm and 4 mm in thickness were modeled using 8-node linear brick C3D8R elements with reduced integration and hourglass control. The finite element mesh presented in Fig. 4 comprises a densely meshed impact zone and a coarse mesh in the other regions. Fixed boundary conditions were defined to the bottom surface of the target similar to the experiment. The projectile was modeled as a rigid body, and a general contact was defined between the projectile and the target with a coefficient of friction set to 0.3. The impact was modeled for an approach angle of 60° and an initial velocity of 110 m/s similar to the experiment. In order to reduce the runtime of the simulation, the spherical projectile was defined just before it comes to contact with the target plate. In order to choose the most appropriate mesh size, a mesh sensitivity analysis was conducted by varying the number of elements from coarse mesh with 1600 elements to fine mesh with approximately 110000 elements and by comparing the maximum displacements given by the models. Based on this analysis, an element size of 0.2 mm was chosen for the finely meshed impact region and an element size of 1.2 mm for the coarse region.

Numerical models that make use of the known elastic–plastic stress–strain behavior of target materials have been shown to be capable of simulating the abrasive wear of materials with sufficient accuracy [32]. In this work, an isotropic plasticity material model based on the stress-strain data obtained from the uniaxial tensile tests conducted at different temperatures was used to represent the steel targets. The elastic Young's modulus was used to describe the stress-strain relation up to the yield stress, while the post-yield behavior was described with the true stress - true plastic strain data shown in Fig. 5 for the different

steels at −60 °C.

3. Results

3.1. Mechanical testing

Table 3 lists the mechanical properties of the test materials, including the yield strength (Rp0.2), ultimate tensile strength (Rm), elongation at fracture (A_5), Charpy impact toughness, and Vickers hardness at the HVPI test temperatures. The ultimate tensile strength (Rm) of all tested materials increased as the temperature decreased. The relative strength increase was the highest for the structural steel S355, which had the lowest strength of the tested materials. At −60 °C its Rm was approximately 25% higher compared to the room temperature value. For the martensitic 400HB and 500HB steels, the increase of strength between room temperature and −60 °C was only 3–5%.

The impact energy values of all test materials determined by Charpy tests [8] are presented also in Fig. 6a. The S355 steel shows a dramatic decrease in the impact toughness between −60 °C and −80 °C, whereas the wear resistant steels, which also at higher temperatures show much lower impact energy values than the structural steel, do not experience such a sudden drop in toughness. The impact toughness values of the 400 H B steel are down to −40 °C clearly higher than those of the 500HB steel. The DBT temperature is between −20 °C and −40 °C. The impact toughness values of the 500HB steel are quite low throughout the entire measurement range. However, it should be noted that the Charpy sample size was only 5 mm × 10 mm x 55 mm, and small sample size generally leads to smaller impact toughness values. There was quite a lot of scatter in the Charpy test results at low temperatures, which especially shows as a winding shape of the S355 impact energy
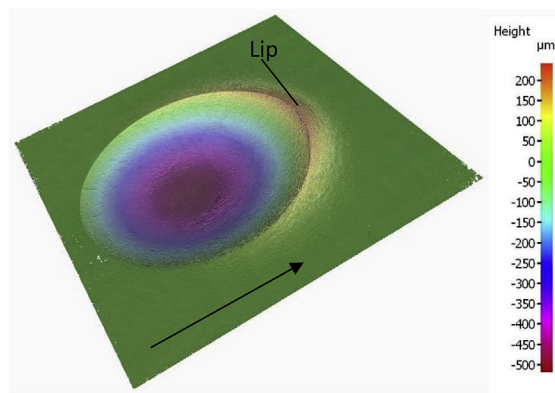
a)
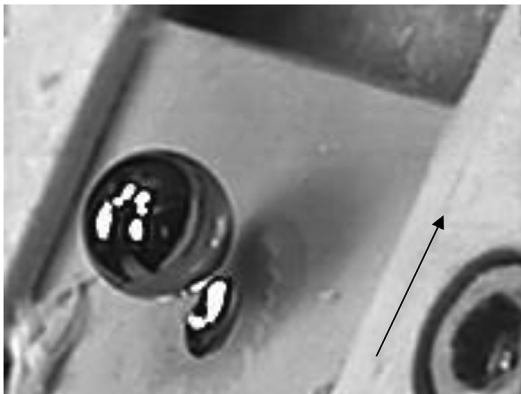
b)
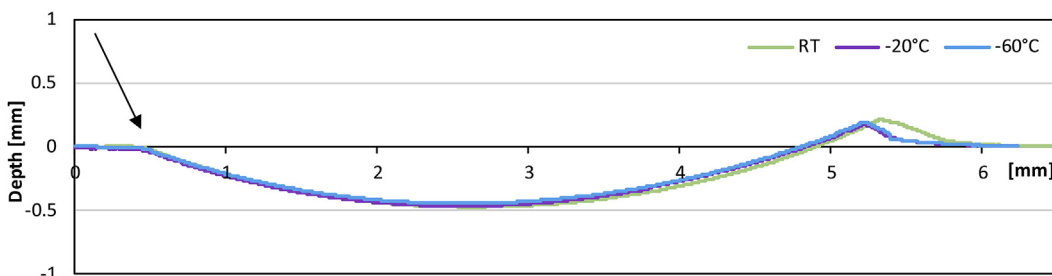
c)

Fig. 7. A) 3D profile of an impact mark in the 400HB steel tested at room temperature, b) snapshot of the impact event at −60 °C, and c) impact crater profiles in the 400HB steel at different test temperatures. The arrows indicate the impact direction.

'curve' between RT and −60 °C.

Fig. 6b shows the low temperature Vickers hardness results for all test materials. Similar to the ultimate strength values, the hardness of all steels increases with decreasing temperature, the increase being over 70 HV10 for the 500HB steel when the temperature decreases from RT to −100 °C.

3.2. Characterization of single impacts

During an impact, the projectile deforms the steel surface markedly. A distinctive lip is formed in the pile-up region, and a sharp ridge appears at the final contact point with the projectile. As an example, Fig. 7a shows the 3D profile of one of the impact marks, and Fig. 7b is a snapshot from a high-speed video recording of the impact event taken immediately after the impact. The amount of plastic deformation decreases with decreasing temperature, which can be seen as a change in
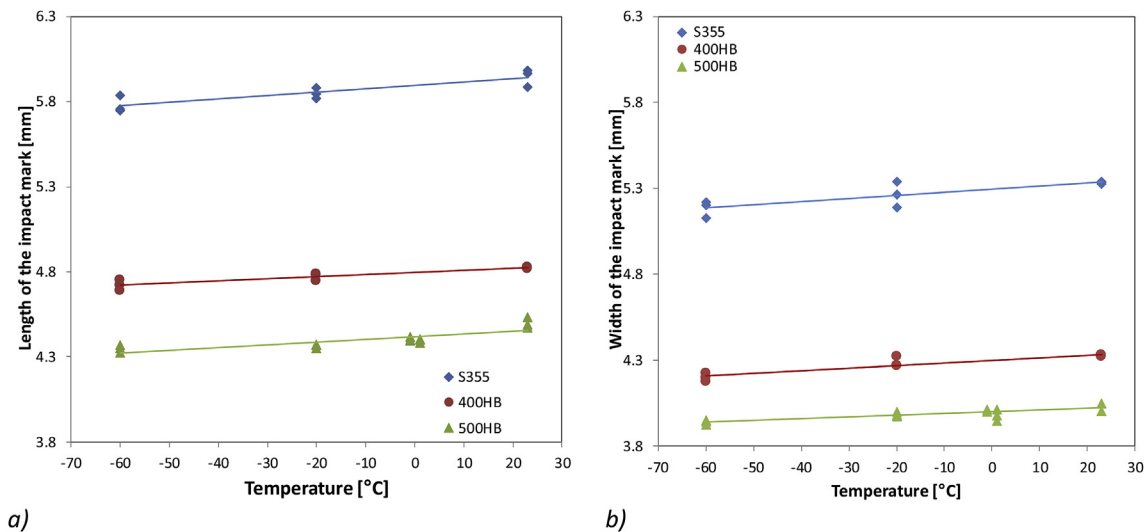
Fig. 8. Measured a) length and b) width of the impact marks of the tested steels at different temperatures.

the form of the lip, as depicted in Fig. 7c.

Supplementary video related to this article can be found at https://doi.org/10.1016/j.triboint.2018.08.016.

The impacts were so severe that they caused the sample sheets to bend slightly. As the determination of the volume loss with a 3D profiler is very sensitive to the flatness of the sample, fracturing of the ridge affected in some cases markedly the obtained volume loss values. Therefore, the dimensional measurements (length and width of the impact mark) with a stereo microscope were found to be a more reliable way of assessing the extent of the surface damage of the samples.

The impact mark length indicates quite well the amount of damage induced in the sample by the impacts of constant impact energy, i.e., by the kinetic energy that the projectile has at the moment of impact. Fig. 8 presents the lengths and widths of the impact marks at the impact test temperatures. There is a distinct but expected difference between the materials, and both dimensions are more or less linearly decreasing with decreasing temperature.

The samples tested at $+1$ °C and -1 °C were also profiled with the Alicona 3D profiling software to see if there are any differences in the mechanisms of material removal from the surface due to the presence of the frost layer. In addition to profiling, the measurements of the length, width and depth of the impact marks were conducted to assess the amount of material ploughed to the sides of the craters. The measurements showed that all the impact mark dimensions were slightly larger at -1 °C, but the difference was smaller than the scatter and thus not statistically significant.

3.2.1. Surface study

In order to better understand the behavior of the studied steels under subzero conditions, the impact marks were characterized by SEM. The martensitic steels 400HB and 500HB behaved quite similarly. Fig. 9 clearly shows that there are significant differences in the surface features found for example in the 400 H B steel samples impacted at

different temperatures. The presented in-lens secondary electron images were taken either about 300 μm from the tip of the impact mark along the centerline of the crater (Fig. 9a, c, and e), or from the center of the impact marks (Fig. 9b, d, and f). In the sample impacted at room temperature, definite marks of abrasion and adhesion can be observed. Even a few tungsten carbide (WC) particles from the projectile, seen as white spots in the image, were attached to the steel surface. At lower temperatures, the grain boundaries and martensite laths of the martensitic steel start to open up, as seen in the center of the impact marks. All these features became clearer with decreasing test temperature. Closer to the exit point of the projectile, i.e., at the tip of the impact mark, also crack formation could be observed at -20 °C and -60 °C. The cracks were circularly distributed to the whole width of the tip. Up to 50 μm long cracks could be identified in the samples (not shown in Fig. 9). At -60 °C, the cracking also initiated the formation of wear particles in the martensitic steels, as seen in Fig. 9e, where micrometer sized particles have been detached from the surface.

The surface microstructures of selected impact marks were etched using Nital to study the position of the cracks and the deformation of surface layer. Although the surface layers were highly deformed, the original microstructural features were still visible in the SEM images seen in Figs. 10 and 11. Fig. 10 shows an example of the opening microstructural features in the 500HB steel and Fig. 11 in the S355 steel after etching of the surface impacted at -60 °C. The etching revealed better the opened lath structures in the martensitic steels and the opened grain boundaries in the ferritic-pearlitic steel. At the center of the impact marks, the microstructure of the steels was visible also in the SEM images (Figs. 9 and 10).

The S355 steel with a ferritic-pearlitic microstructure behaved in the impacts quite similarly to the martensitic steels, but the microstructure was visible already from the polished surface with SEM. However, at the bottom of the impact mark, the differences in the appearance between the ferritic and pearlitic areas were evident as seen in
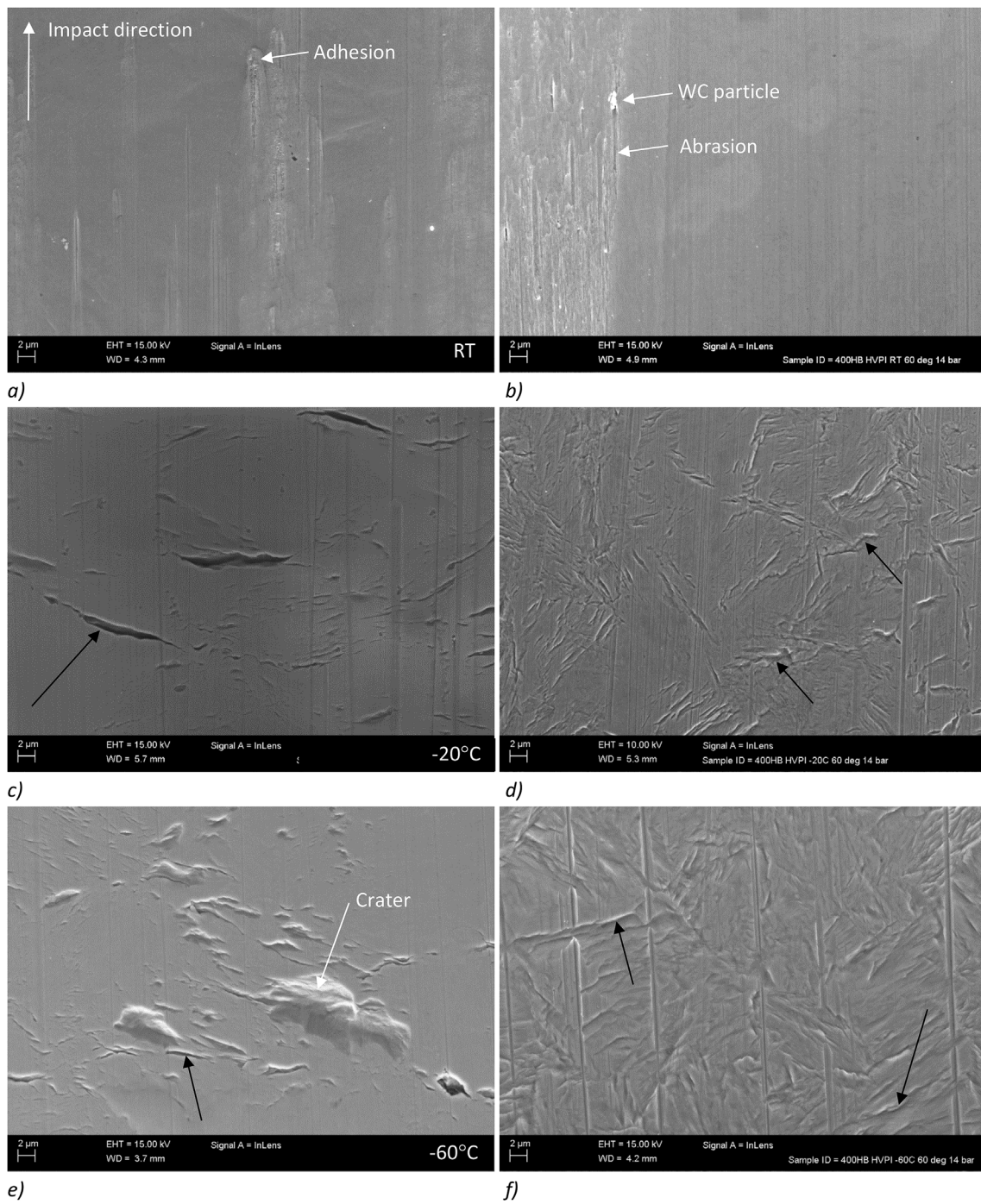
Fig. 9. SEM images from the impact surface of the 400HB steel tested at a-b) RT, c-d) −20 °C, and e-f) −60 °C. Images a, c, and e are taken close to the top of the impact mark, and images b, d, and f from the center of the impact mark. The black arrows indicate opening of the microstructural features. The impact direction is the same in all images.
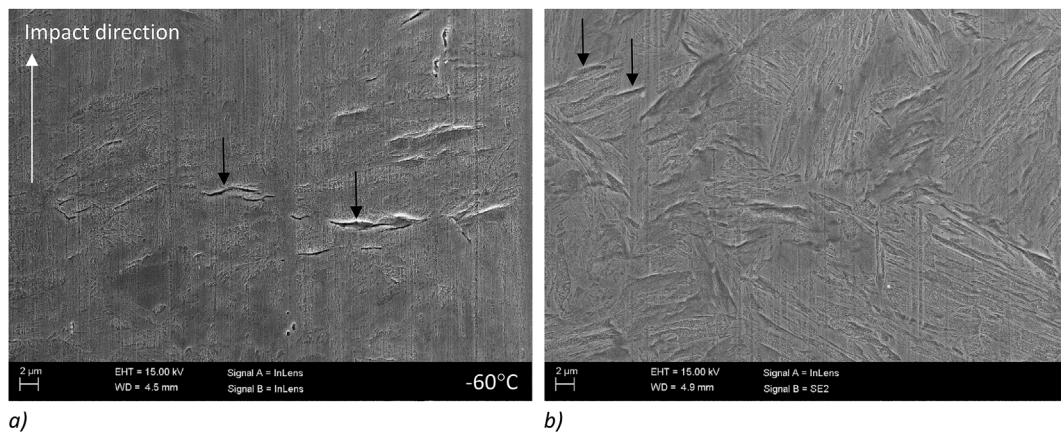
Fig. 10. SEM images from the 500HB steel tested at −60 °C and etched with Nital a) close to the tip of the impact mark and b) at center of the impact mark. The arrows indicate some of the opened microstructural features. The impact direction is the same in Figs. 10–12.
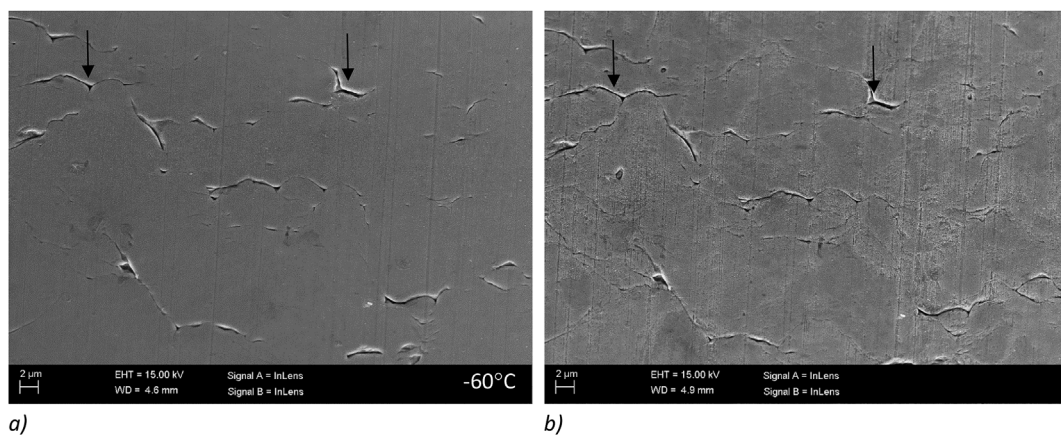

Fig. 11. SEM images from the S355 steel tested at −60 °C showing wear close to the tip of the impact mark a) unetched and b) etched from the same area. The arrows indicate some of the opened grain boundaries.
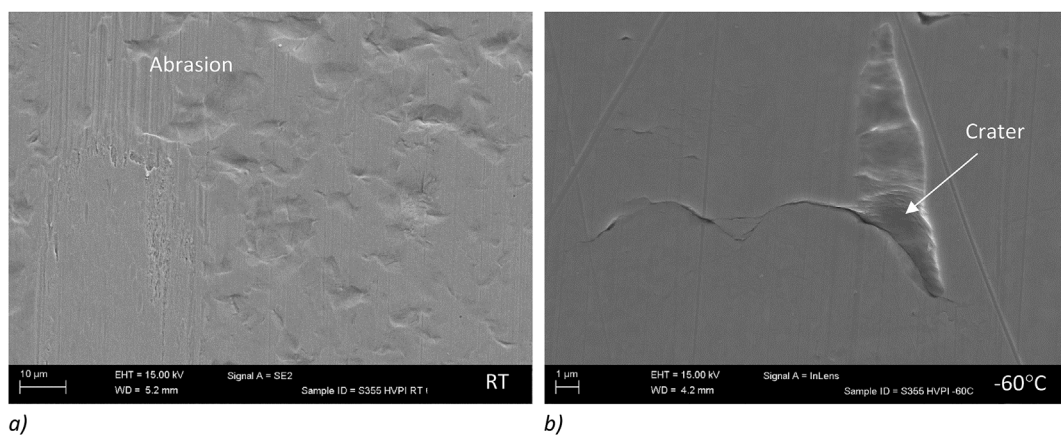

Fig. 12. SEM images from the S355 steel showing a) the microstructure at the center of the impact mark at RT, and b) wear close to the tip of the impact mark at −60 °C.

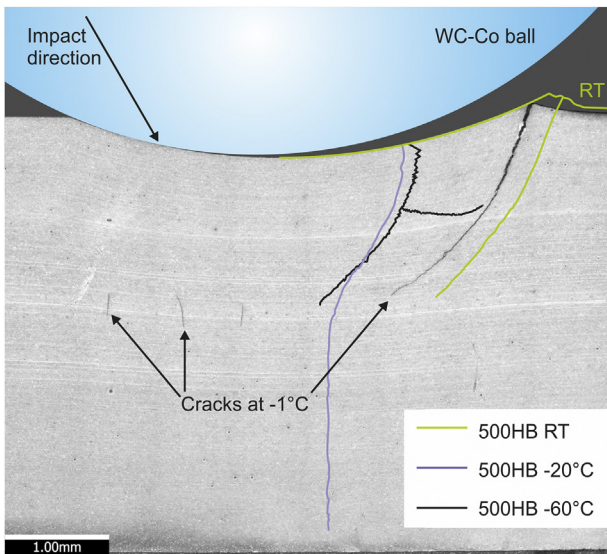**Fig. 13.** Optical micrograph showing the cross section of an impact mark in the 500HB steel tested at −1 °C, and the formation of cracks in the 500 H B steel at various temperatures.

Fig. 12a. Moreover, clear adhesion marks and scratches were observed on the impact mark surfaces at room temperature, and cracking-induced wear started to happen already at −20 °C, with wear particles up to 20 μm in size being detached from the surface. Fig. 12b illustrates a typical wear damage in a S355 sample tested at −60 °C.

There was no visible difference between the impact mark surfaces of the 500HB samples tested at +1 °C and −1 °C. This means that the ice formed on the sample surface did not have a significant effect on the impact response of the sample. The opening of the martensite laths was visible at both temperatures in the center areas of the impact marks.

3.2.2. Cross section study

The cross sections revealed that only the 500HB samples had experienced extensive cracking during the impacts. Both subsurface cracks as well as cracks extending to the surface were observed over the entire studied temperature range. Fig. 13, which combines single cross-section images from samples tested at four temperatures, shows that in the 500HB samples tested at lower temperatures the cracks were positioned inside the impact mark area rather than at the top of the pile-up ridge, as in the samples impacted at RT and around 0 °C. In the samples tested at 1 °C and −1 °C, short transgranular cracks had also

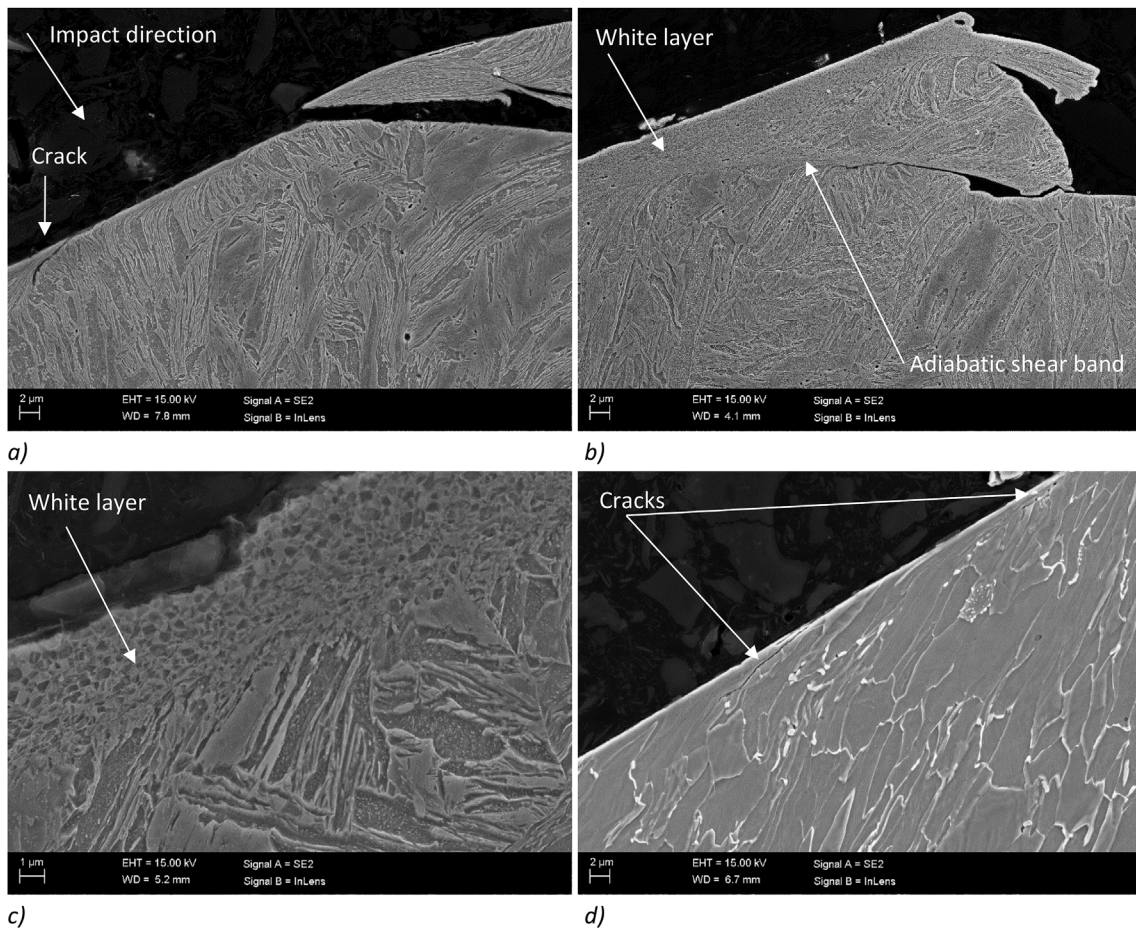**Fig. 14.** SEM images of the cross sections of the impact mark ridges of a) 400HB and b, c) 500HB steels tested at −60 °C and d) S355 steel tested at −20 °C. The impact direction is the same in all images.
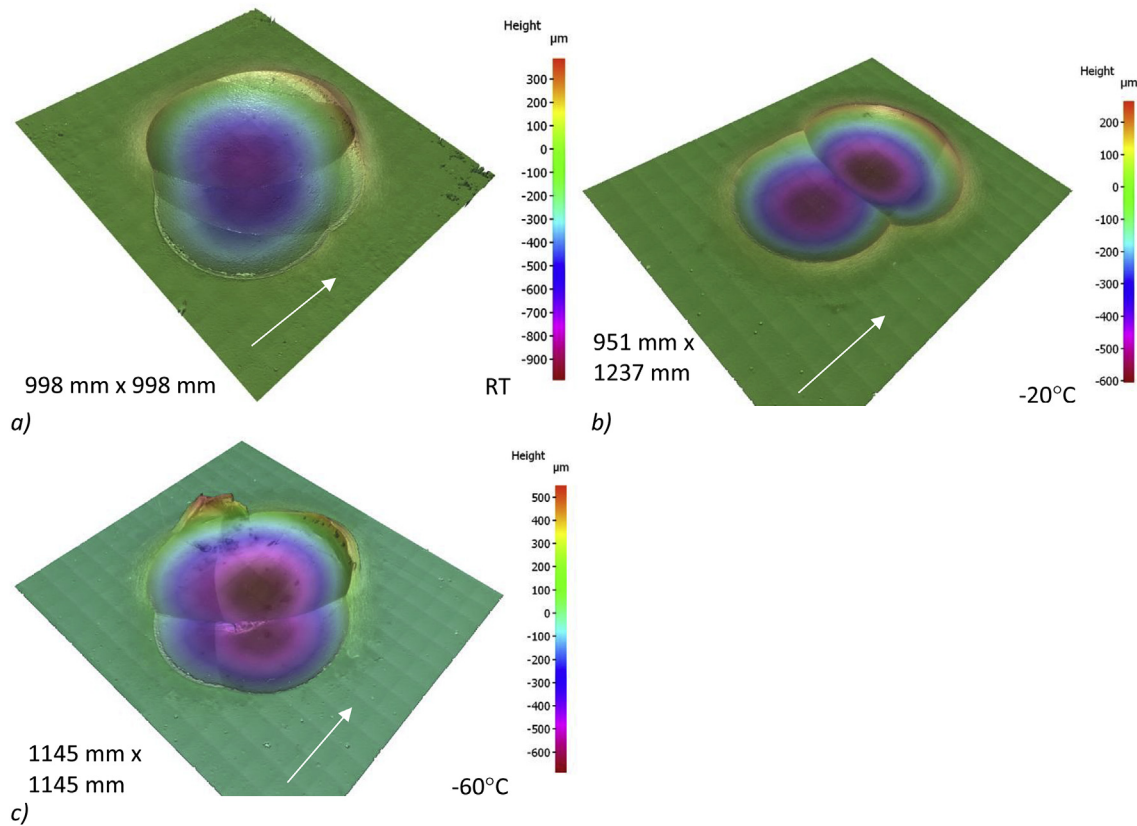
Fig. 15. 3D profiles of five partially overlapping impact marks in the 500HB steel tested at a) room temperature, b) −20 °C, and c) −60 °C. The arrows indicate the impact direction.

formed in the centerline of the impact zone. Moreover, the deformation of the steel was visible down to 3 mm below the surface as seen in Fig. 13.

Fig. 14a and b illustrate the deformation and cracking in the ridge tip areas in the 400HB and 500 H B samples tested at −60 °C. In the 400HB steel, the cracks were formed in the so-called white layer or a thin shear band layer in the surface region of about 100 μm from the tip of the ridge. In the 500HB steel, the slightly cracked white layer extended down to 300 μm from the top of the impact mark, i.e., further than seen in Fig. 14b. Fig. 14c shows the very fine microstructure of the white layer formed in the 500HB steel. The thickness of the white layer was about 6 μm. Moreover, an adiabatic shear band was formed in the shear localization area at the tip of the ridge, and the sample was fractured along it.

In the 400HB samples tested under subzero conditions, also small intergranular cracks were formed in the pile-up region, the shape and size of which was changing with temperature, as was seen already in Fig. 9 c and e. In the samples impacted at room temperature, the lip extended wider and with a smoother shape in comparison to the lips formed at lower temperatures. The same change was seen also in the 500 H B steel samples.

In the cross-sections of the S355 samples, small single subsurface cracks parallel to the impact mark surfaces with a length of

approximately 100 μm were detected in the samples tested below 0 °C. Moreover, there were smaller cracks close to the tip of the impact mark (Fig. 14d). The impact marks were so deep that small bulges were visible also on the rear side of the 4 mm steel plates.

3.3. Characterization of multiple impacts

Some of the 500HB steel samples were impacted multiple times in order to see the effect of repeated impacting on the deformation of the surfaces. Even though the HVPI device is quite precise, the individual impact marks did not fully coincide, as seen in Fig. 15. Nevertheless, the differences between the samples tested at different temperatures were found to increase markedly, as seen in Fig. 16, which presents some typical features of the overlapping impact marks. At room temperature, the forming craters were only plastically deformed and no cracking was observed. Moreover, the multiple impacted surfaces contained signs of abrasion similar to the single impact marks. At −20 °C, some cracks were already formed, but at −60 °C the crack formation was severe and the steel surface started to fracture in a brittle manner. The largest fracture on the edge of the impact area was almost 2 mm long, as seen in Fig. 16d.

Although cracking on the surfaces was barely visible, especially on samples tested at room temperature, the cross-sections of the samples
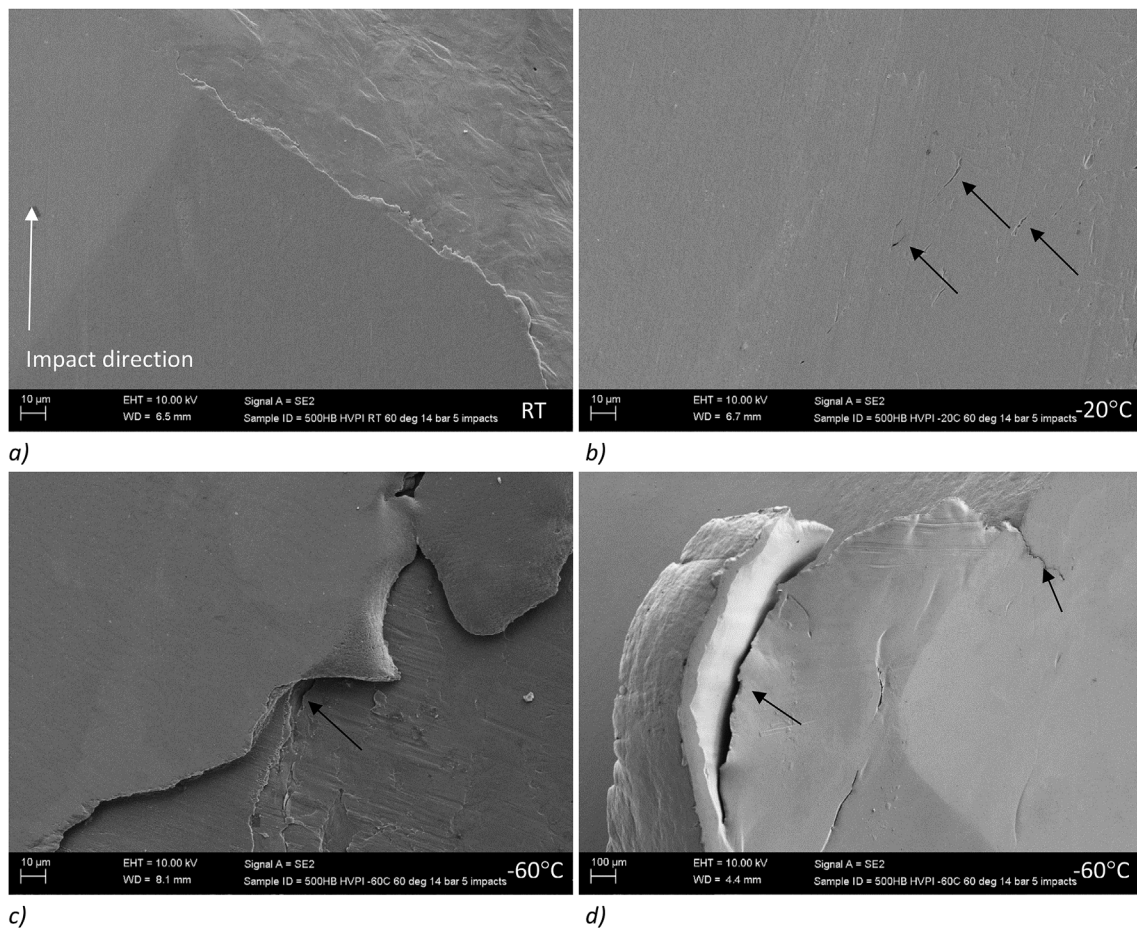
Fig. 16. SEM images of the 500HB steel samples showing some typical features of overlapping impact marks from tests conducted at a) RT, b) −20 °C, and c, d) −60 °C. The black arrows indicate examples of cracking sites. The impact direction is the same in all images.
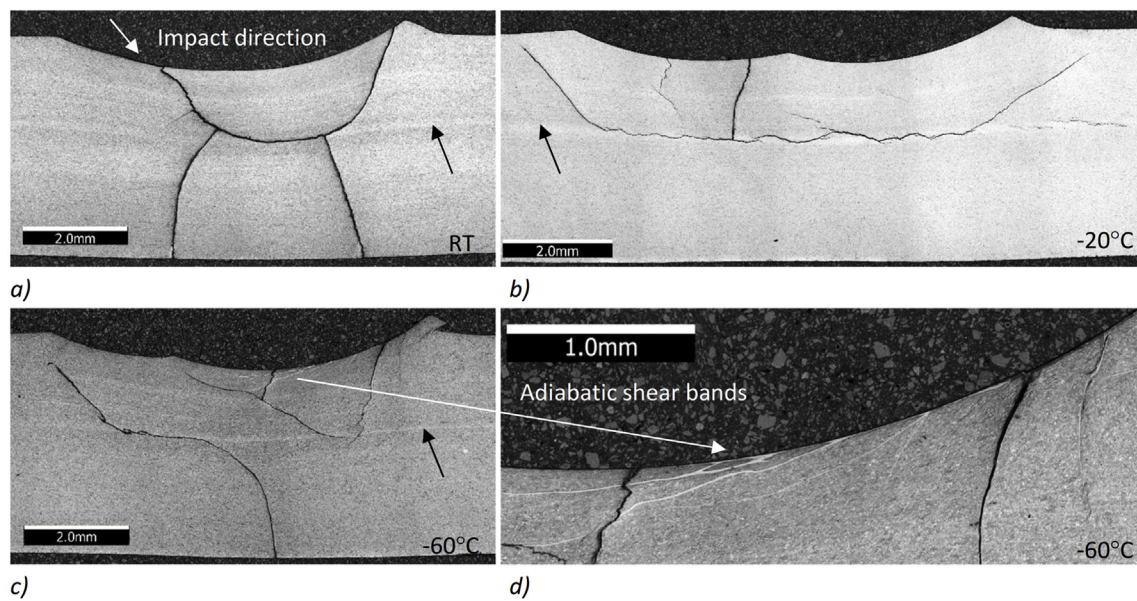

Fig. 17. Optical micrographs of the cross-sections of five partially overlapping impact marks in the 500HB steel tested at a) room temperature, b) −20 °C, and c) −60 °C with d) adiabatic shear bands indicated by the white arrow. The black arrows indicate the centerline segregation. The impact direction is the same in all images.
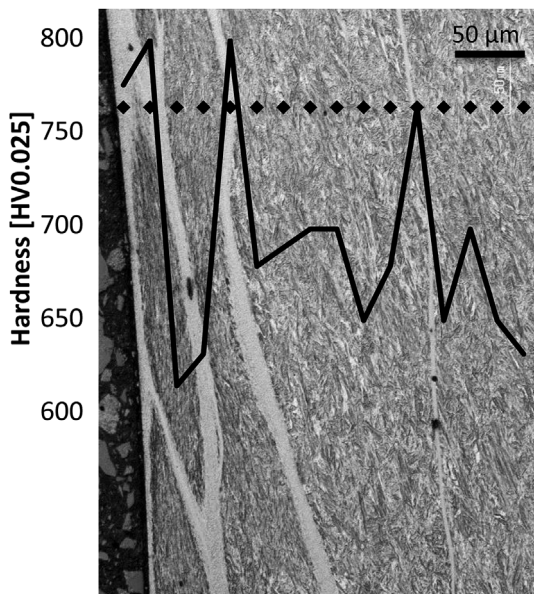
Fig. 18. Optical micrograph of the adiabatic shear bands formed in the 500HB steel at $-60\,°C$. The hardness profile was measured from the diamond marker locations.

revealed severe cracking in all samples, as disclosed by Fig. 17. The largest cracks followed the centerline segregation, which is seen as a lighter line in the etched cross-section of the steel plate. In the centerline the steel hardness was quite high, $688 \pm 13\ HV_{0.1}$, while the average hardness of the plate was $506.5 \pm 6.5\ HV_{10}$.

Only at the testing temperature of $-60\,°C$, a significant number of adiabatic shear bands (ASB) were formed. Fig. 18 presents a typical example of the adiabatic shear bands with a hardness profile, the mean hardness of the thick adiabatic shear bands being $787 \pm 14\ HV_{0.025}$. At $-60\,°C$, the thickness of a single ASB was typically under $15\,\mu m$. At $-20\,°C$, just a couple of thin, less than $5\,\mu m$ thick ASBs were observed.

3.4. Results of the FE simulation of HVPI

Fig. 19 shows the typical sequence of events when a spherical projectile hits a steel plate, as simulated by the Abaqus/Explicit Finite Element software. In the beginning of the contact, the projectile deforms the target plastically at the point of impact and starts to create a crater on the surface by displacing the material in front of it (b-d). When the projectile starts to bounce back (e-f), it leaves behind a lip of material at the exit point. A close-up of the impact crater at the end of the simulation is shown in Fig. 19g.

One of the advantages of the numerical modeling is that it can provide us with a good estimate of the force(s) acting on the steel surface during the impact, which is quite difficult to experimentally measure (although such experiments with the HVPI device have in fact already been done [18]). Fig. 20 shows the simulated time history of the contact force during an impact of a WC-Co projectile on a 500HB steel target at the speed of $110\,m/s$ at $-60\,°C$. It can be seen that the

contact duration of the impact is about $37\,\mu s$, and the peak force is $32.5\,kN$. The evolution of the impact crater during the impact is illustrated in Fig. 21.

The Abaqus model was validated by comparing the simulated profiles of the impact craters taken along their centerline both in the longitudinal and transverse directions with the 3D profilometer results. As Fig. 22 illustrates, the FE simulation is able to reproduce quite well the plastic deformation related to the ploughing process during the impact. The maximum depth of the craters were especially well predicted by the simulations for all studied steels at all studied temperatures. The lengths and widths of the craters were also closely similar in the experiments and simulations. However, the height of the lip at the end of the crater was always over-estimated in the simulations. One reason for this discrepancy evidently is that in the real experiments some material is always lost through chip formation, as seen for example in Fig. 14, while there is no element deletion or damage included in the model to take account of such events. However, the observed discrepancy appears to be too large to be explained only by missing chip formation in the model. Another possible reason could be the missing ASB formation in the model, affecting the hardening behavior and size of the forming lip.

4. Discussion

Detailed knowledge of the behavior of steels at subzero temperatures enhances the material selection especially for the Arctic environments. In general, the properties known to improve the wear resistance, such as hardness and strength, should be as high as possible while retaining sufficient ductility to minimize the risk of a catastrophic (brittle) failure. In the current tests, the dimensions of the impact marks decreased with the increasing ultimate tensile strength and decreasing temperature. Fig. 23 illustrates the quite linear correlation between the measured impact mark dimensions and the strength of the steels at the applied test temperatures.

The increased strength with decreasing temperature was found to induce the formation of adiabatic shear bands in the martensitic steel samples impacted at $-60\,°C$. The nanostructured ASB layers prove that the steel had been deformed above the critical strain rate of the steel [33]. The formation of the adiabatic shear bands also seems to facilitate the crack formation especially in the case of multiple impacts, as seen in Fig. 24 and also reported in many earlier studies [21,23,24,34]. According to Kim et al. [34], in the Charpy impact tests the ASBs follow the maximum shear stress planes, and the results of the current multiple impact tests indicate the same. Moreover, Kim et al. [34] noted that tempering of the steel at $600\,°C$ producing martensitic structure with high carbide volume prevented the formation of ASBs in dynamically compressed samples. Thus, it is possible to develop steels that are less prone to form ASB's. Fig. 24a shows that in addition to the cracked subsurface ASBs, a thin white layer was formed on the impact surface of the samples tested at $-60\,°C$. Fig. 24b also reveals the nanostructure of the ASB layer. Lindroos et al. [18] reported cracking of the ASB layers in martensitic steels already during single impacts, but the multiple impacts used in this work probably further enhanced the effect. Similar cracked ASBs are formed also in the actual impact wear conditions, as recently reported by Abbasi et al. [23] for the steel scrap shear blades,
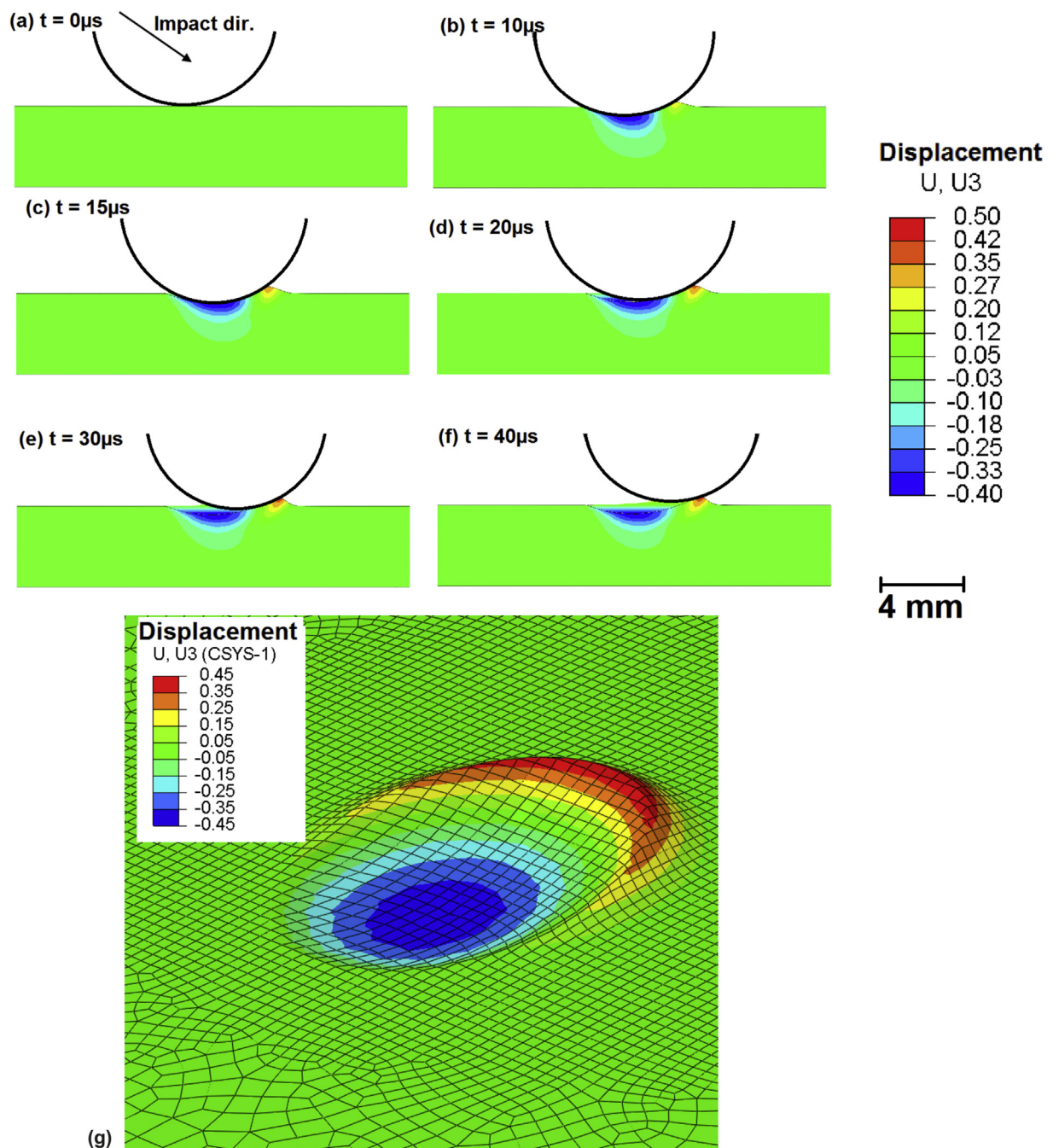
Fig. 19. Typical simulated sequence of events during a high-speed impact of a ball with a tilted steel plate sample.
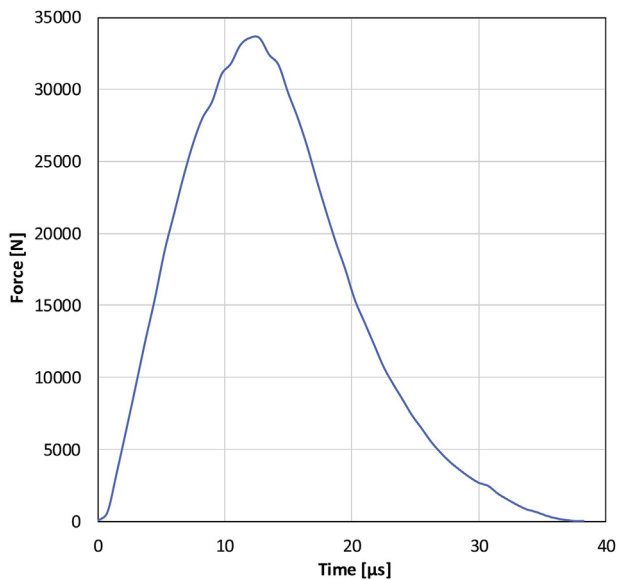
Fig. 20. Force-time history of the impact on a 500HB steel target at the speed of 110 m/s at −60 °C.

the temperature effects due deformation heating, including the formation of ASBs, would be included in the further modeling schemes of the HVPI tests. The addition of appropriate failure criteria would also increase the accuracy of the simulations markedly. Therefore, FE analysis with modified Johnson Cook model that includes temperature and strain rate dependency, as well as toughness of the material measured from Charpy tests to capture the energy absorption behavior, is proposed for future study.

In the RT tests, the impact marks showed clear indications of both adhesion and abrasion (Fig. 9 a and b). Although the impact angle was steep, 60°, the WC-Co ball ploughed the steel surfaces and even some WC particles were embedded to the steel. However, when the test temperature was decreased, the contact surfaces showed mainly marks of abrasion in the form of linear scratches and the amount of adhesion marks diminished (Fig. 9 c–f). In the tests close to 0 °C, the thick ice layer formed on the sample surface due to ambient humidity seemed to have essentially no effect on the dimensions of the impact marks. This could be explained by the melting of the ice layer formed on the sample immediately when the impactor hits the steel surface [15].

At subzero temperatures, the small surface cracks in the top part of the impact marks led to material removal from the surface of all tested steels. This cracking was not caused by adiabatic shear bands, because the white layers were formed only at the very tips of the ridges, and these cracks were found a bit further away from those areas. In the center of the impact marks, the microstructure of the martensitic steels was clearly visible at subzero temperatures. Apparently, polishing of the samples before testing already revealed the microstructure of the steels, i.e. slightly highlighted the harder phases. Then the deformation due to the impact further opened the structure between the laths, the lath packets, and the grain boundaries. These features have multiple orientations in the martensitic structure [31,35], and under deformation at subzero temperatures, they start to lose their structural integrity. Thus, the presented images appear to reveal the first steps towards a more detrimental failure during impact loading. In the further studies, it would be interesting to study the evolution of the failure by characterization of the impacts marks after every impact in the multiple impact tests.

5. Conclusions

The effects of subzero temperatures on the response of three steels to single and multiple oblique angle impacts were studied. From the
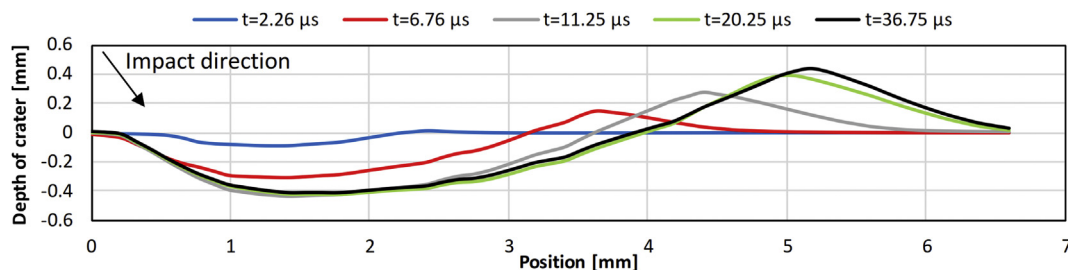
where ASBs were formed both on the wear surface as well as in the subsurface similar to the multiple impact tests of this work. Although the surface study showed cracking only at −60 °C, all multiple impacted samples were severely cracked, as observed in the cross-sectional studies. However, as the impacts had visibly bent the steel plates, it is also possible that the cracking had partly occurred only during cutting of the microscopy specimens, when the residual stresses formed during impacting had been released.

However, not all the cracks were initiated by the adiabatic shear bands, and especially in the 500HB steel, also 'ordinary' subsurface cracking occurred at all testing temperatures both in single and multiple impact tests. Similar behavior could also be observed in the FE simulated impacts, even though the model does not take account of the adiabatic effects or particular features of the microstructure. Fig. 25 shows that the cross-section of the simulated target contains a high concentration of shear strains in the same region where the cracks were observed in the physical experiments (Fig. 13). It is recommended that

Fig. 21. Evolution of the impact crater during an impact on the 500HB steel at −60 °C.
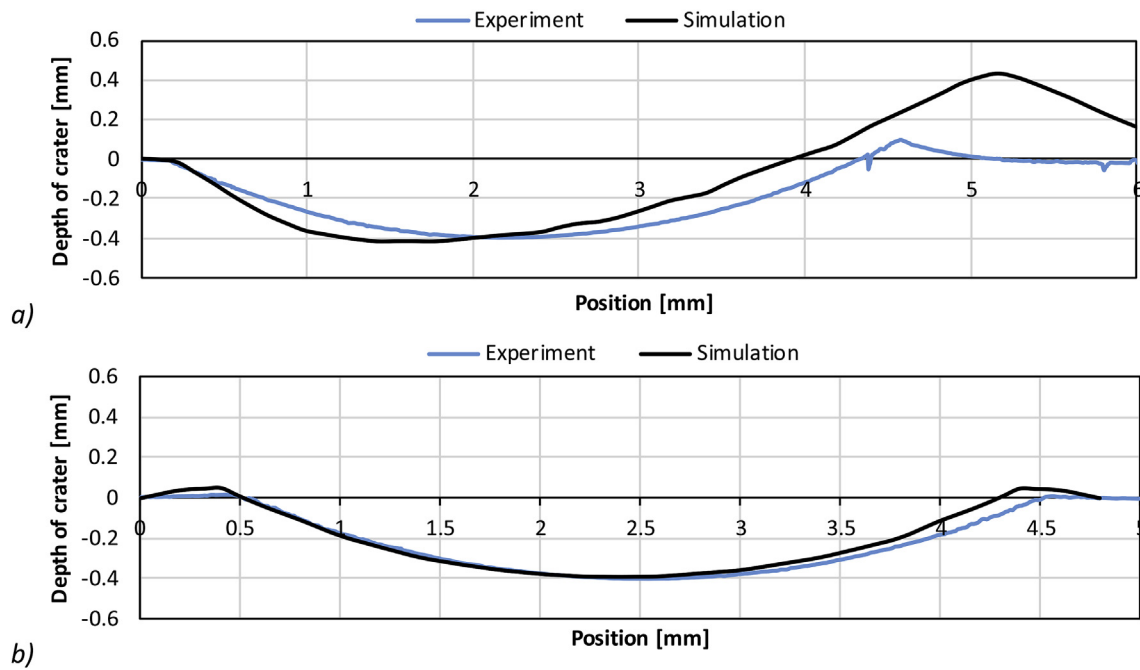
Fig. 22. Comparison of the experimental and simulated crater profiles in a) longitudinal and b) transverse directions for a 500HB steel impact tested at −60 °C.
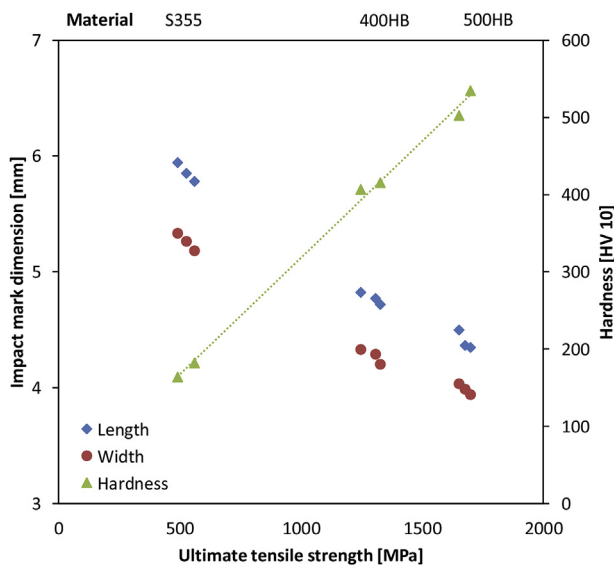

Fig. 23. Measured length and width of the impact marks and hardness vs. ultimate tensile strength of the tested steels at the applied test temperatures.

results, the following conclusions could be drawn:

- At temperatures from RT down to −60 °C, the degree of deformation of the studied steels in single impacts correlate well with the ultimate tensile strength of the steels.
- In martensitic steels, decreasing temperatures promote the formation of adiabatic shear bands.
- During multiple impacts at −60 °C, ample formation of subsurface adiabatic shear bands facilitates the initiation of cracking.
- In single impact tests at subzero temperatures, cracking along various microstructural features, such as grain boundaries and martensite laths, leads to material removal in all tested steels near the tip of the impact mark. Moreover, plastic deformation initiates the opening of the martensite laths at the bottom of the impact marks.
- The high velocity particle impactor with liquid nitrogen cooling was proven an excellent test system for controlled oblique angle impact wear tests at low temperatures, complementing the data collected by other mechanical testing systems.
- A Finite Element model with a simple elastic-plastic material law was capable of reproducing the plastic deformation and crater formation observed in the steel targets during high-speed impacts.
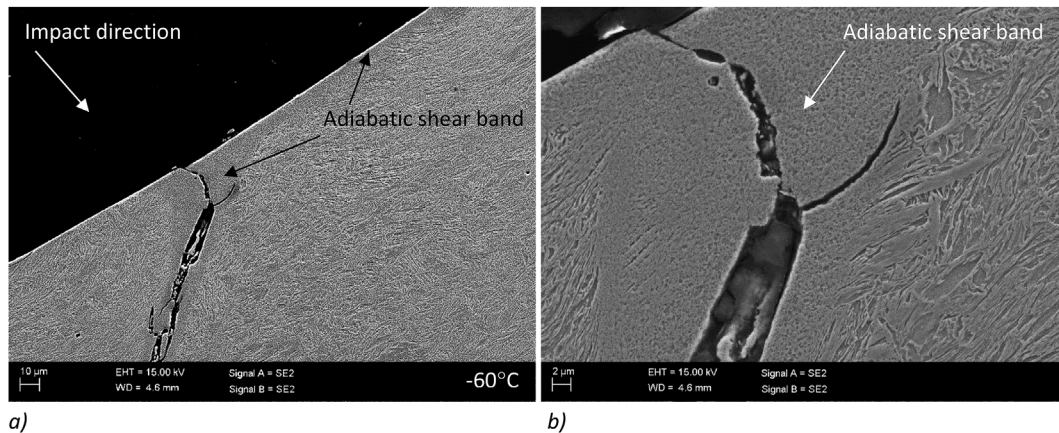
Fig. 24. SEM images of the cross-sections of five partially overlapping impact marks in the 500HB steel tested at −60 °C, showing cracks following the path of adiabatic shear bands (b enlarged from a).
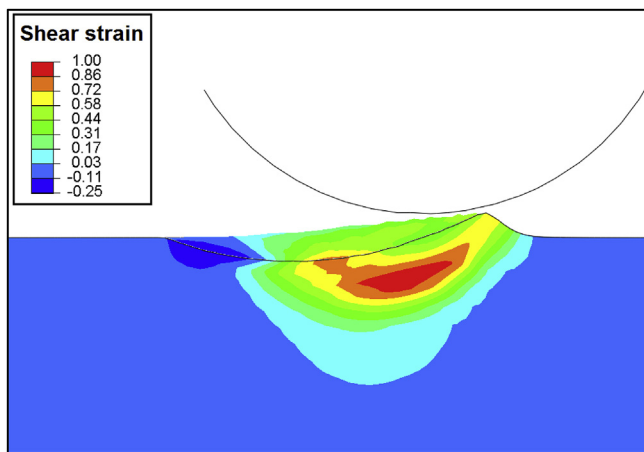

Fig. 25. Cross-sectional view of shear strain distribution in the 500HB steel target after an impact at 110 m/s at −60 °C, revealing high subsurface stresses. The thin black line indicates the bottom of the impact mark at the plane of the cross-section.

Acknowledgements

Appendix A. Supplementary data

Supplementary data related to this article can be found at https://doi.org/10.1016/j.bbrc.2016.12.032.

References

[1] Zlotnikov D. Mining in the extreme. Cim Mag 2012:50–6http://issuu.com/cim-icm_publications/docs/aug12_finald_lr.

[2] Epstein EJ. The rise and fall of diamonds. Smashwords; 2011.

[3] Harris MD, Grogg WJ, Akoma A, Hayes BJ, Reidy RF, Imhoff EF, et al. Revisiting (some of) the lasting impacts of the liberty ships via a metallurgical analysis of rivets from the SS "John W. Brown,". JOM (J Occup Med) 2015;67:2965–75. https://doi.org/10.1007/s11837-015-1668-1.

[4] Layus P, Kah P, Ryabov V, Martikainen J. Evaluation of applicability of thick E500 TMCP and F500W QT steel plates for Arctic service. Int J Mech Mater Eng 2016;11:4. https://doi.org/10.1186/s40712-016-0057-z.

[5] Yan J-B, Xie J. Experimental studies on mechanical properties of steel reinforcements under cryogenic temperatures. Construct Build Mater 2017;151:661–72. https://doi.org/10.1016/j.conbuildmat.2017.06.123.

[6] Yan JB, Liew JYR, Zhang MH, Wang JY. Mechanical properties of normal strength mild steel and high strength steel S690 in low temperature relevant to Arctic environment. Mater Des 2014;61:150–9. https://doi.org/10.1016/j.matdes.2014.04.057.

[7] Layus P, Kah P, Martikainen J, Pirinen M, Khlushova E, Ilyin A. European and Russian metals for arctic offshore structures. Proc Twenty-Third Int Offshore Polar Eng 2013;9:242–9.

[8] SFS-EN ISO 148-1. Metallic materials. Charpy pendulum impact test. Part 1 : test method, 2009, 30. 2009.

[9] ASTM. E208 - 17e1 Standard Test Method for Conducting Drop-Weight Test to Determine Nil-Ductility Transition Temperature of Ferritic Steels. 2017. p. 14. https://doi.org/10.1520/E0208-17E01.

[10] Hokka M, Kuokkala V-T, Curtze S, Vuoristo T, Apostol M. Characterization of strain rate and temperature dependent mechanical behaviour of TWIP steels. J Phys IV Fr 2006;134:1301–6. https://doi.org/10.1051/jp4:2006134197.

[11] Hokka M, Curtze S, Kuokkala V-T. Tensile HSB testing of sheet steels at different temperatures. Proc. 2007 SEM Ann. Conf. Expo. Exp. Appl. Mech. 2007. paper 250.

[12] Curtze S, Kuokkala VT, Hokka M, Peura P. Deformation behavior of TRIP and DP steels in tension at different temperatures over a wide range of strain rates. Mater Sci Eng 2009;507:124–31. https://doi.org/10.1016/j.msea.2008.11.050.

[13] Subramonian B, Basu B. Development of a high-speed cryogenic tribometer: design concept and experimental results. Mater Sci Eng 2006;415:72–9. https://doi.org/10.1016/J.MSEA.2005.09.086.

[14] Basu B, Mukhopadhyay A, Mishra A, Sarkar J. Does thermal conductivity play a role in sliding wear of metals in cryogenic environment? J Tribol Asme 2010;132:1–5. https://doi.org/10.1115/1.4002503.

[15] Lyu Y, Bergseth E, Olofsson U. Open system tribology and influence of weather condition. Sci Rep 2016;6. https://doi.org/10.1038/srep32455.

[16] Ma L, Shi LB, Guo J, Liu QY, Wang WJ. On the wear and damage characteristics of rail material under low temperature environment condition. Wear 2018;394–395:149–58. https://doi.org/10.1016/J.WEAR.2017.10.011.

[17] Ratia V, Lindroos M, Valtonen K, Apostol M, Kuokkala V. Impact behavior of martensitic steel at low temperatures. Nord. Conf. Proc. Hämeenlinna: VTT; 2016. p. 1–9.

[18] Lindroos M, Apostol M, Kuokkala V-T, Laukkanen A, Valtonen K, Holmberg K, et al. Experimental study on the behavior of wear resistant steels under high velocity single particle impacts. Int J Impact Eng 2015;78:114–27. https://doi.org/10.1016/j.ijimpeng.2014.12.002.

[19] Hossain R, Pahlevani F, Witteveen E, Banerjee A, Joe B, Prusty BG, et al. Hybrid structure of white layer in high carbon steel - formation mechanism and its properties. Sci Rep 2017;7:1–12. https://doi.org/10.1038/s41598-017-13749-7.

[20] Odeshi AG, Bassim MN. Evolution of adiabatic shear bands in a dual-phase steel at very high strain rates. Mater Sci Eng 2008;488:235–40. https://doi.org/10.1016/j.msea.2007.11.021.

[21] Boakye-Yiadom S, Bassim MN. Effect of prior heat treatment on the dynamic impact behavior of 4340 steel and formation of adiabatic shear bands. Mater Sci Eng 2011;528:8700–8. https://doi.org/10.1016/j.msea.2011.08.036.

[22] Nikas GK. Modeling dark and white layer formation on elastohydrodynamically lubricated steel surfaces by thermomechanical indentation or abrasion by metallic particles. J Tribol 2015;137:031504. https://doi.org/10.1115/1.4029944.

[23] Abbasi E, Luo Q, Owens D. Case study: wear mechanisms of NiCrVMo-steel and CrB-steel scrap shear blades. Wear 2018;398–399:29–40. https://doi.org/10.1016/j.wear.2017.11.014.

[24] Zhang B, Shen W, Liu Y, Tang X, Wang Y. Microstructures of surface white layer and internal white adiabatic shear band. Wear 1997;211:164–8. https://doi.org/10.1016/S0043-1648(97)00099-9.

[25] Fang L, Cen Q, Sun K, Liu W, Zhang X, Huang Z. FEM computation of groove ridge and Monte Carlo simulation in two-body abrasive wear. Wear 2005;258:265–74. https://doi.org/10.1016/j.WEAR.2004.09.024.

[26] Kivikytö-Reponen P, Laukkanen A, Apostol M, Waudby R, Andersson T, Helle A, et al. Modelling and testing of elastomer impact deformation under high strain rates. Tribol Mater Surface Interfac 2014. https://doi.org/10.1179/1751584X14Y.

0000000067.

[27] Arias A, Rodríguez-Martínez JA, Rusinek A. Numerical simulations of impact behaviour of thin steel plates subjected to cylindrical, conical and hemispherical non-deformable projectiles. Eng Fract Mech 2008;75:1635–56. https://doi.org/10.1016/j.engfracmech.2007.06.005.

[28] Iqbal MA, Senthil K, Madhu V, Gupta NK. Oblique impact on single, layered and spaced mild steel targets by 7.62 AP projectiles. Int J Impact Eng 2017;110:26–38. https://doi.org/10.1016/j.ijimpeng.2017.04.011.

[29] Cho S, Truong DD, Shin HK. International Journal of Impact Engineering Repeated lateral impacts on steel beams at room and sub-zero temperatures. Int J Impact Eng 2014;72:75–84. https://doi.org/10.1016/j.ijimpeng.2014.05.010.

[30] Apostol M, Kuokkala V-T, Laukkanen A, Holmberg K, Waudby R, Lindroos M. High velocity particle impactor – modeling and experimental verification of impact wear tests. World tribol. Congr., torino, Italy. 2013. p. 1–4.

[31] Lindroos M, Ratia V, Apostol M, Valtonen K, Laukkanen A, Molnar W, et al. The effect of impact conditions on the wear and deformation behavior of wear resistant steels. Wear 2015;328–329:197–205. https://doi.org/10.1016/j.wear.2015.02.032.

[32] Woldman M, Van Der Heide E, Tinga T, Masen MA. A finite element approach to modeling abrasive wear modes. Tribol Trans 2017;60:711–8. https://doi.org/10.1080/10402004.2016.1206647.

[33] Xu Y, Meyers MA. Nanostructural and microstructural aspects of shear localization at high-strain rates for materials. Adiabatic shear localization 2012. p. 111–71. https://doi.org/10.1016/B978-0-08-097781-2.00003-4.

[34] Kim H, Park J, Kang M, Lee S. Interpretation of Charpy impact energy characteristics by microstructural evolution of dynamically compressed specimens in three tempered martensitic steels. Mater Sci Eng 2016;649:57–67. https://doi.org/10.1016/j.msea.2015.09.099.

[35] Ratia V, Rojacz H, Terva J, Valtonen K, Badisch E, Kuokkala V-T. Effect of multiple impacts on the deformation of wear-resistant steels. Tribol Lett 2015;57. https://doi.org/10.1007/s11249-014-0460-7.